Title

The cold-inducible RNA-binding protein RBM3 stabilises viral mRNA at the cooler temperatures of the upper respiratory tract.

Authors

Hannah L Coutts[1], Hannah L Turkington[1], Stefano Bonazza[1], Erin M P E Getty[1], Swathi Sukumar[1], Ultan F Power[1], David G Courtney[1]

Affiliations

1 Wellcome-Wolfson Institute for Experimental Medicine, Queen's University Belfast, Belfast BT9 7BL, UK

Abstract

Temperature regulation is a key aspect of homeostasis, and several systems are involved in orchestrating adjustments in gene expression at the cellular level. One such factor is RBM3, a cold-inducible RNA-binding protein implicated in several aspects of mRNA processing and regulation. The upper respiratory tract serves as a unique environment regarding temperature regulation. Physiologically, the lower tract is relatively stable at 37°C, while the upper tract fluctuates at or below 33°C. Adapting to this temperature differential, and the subsequent differences in transcriptome and proteome, is essential for respiratory viruses that infect and cause disease in the lower tract while simultaneously replicating and transmitting from the upper tract. At present, our understanding of the molecular mechanisms underlying influenza virus infection at cooler temperatures is lacking. Unsurprisingly, RBM3 protein levels are highest in nasopharyngeal tissue. Coupled with its known role in positively regulating bound RNA, it is an appealing candidate for manipulation by respiratory viruses. We found siRNA knockdown of RBM3 significantly decreased viral replication. To disentangle the direct effect of RMB3 from the shift in global gene expression at colder temperatures, we generated an A549 cell line constitutively overexpressing RBM3 at 37°C. Overexpression resulted in a significant increase in levels of viral replication. RBM3 was found to readily bind viral NP mRNA during infection and prolong the half-life of these transcripts. In contrast, an RBM3 RNA binding null mutant reverses this phenotype, validating that direct interaction of RBM3 has a stabilising effect on viral transcripts. The proviral nature of increased RBM3 levels was further validated in the more clinically relevant model of well-differentiated primary nasal epithelial cells. These data suggest a role for RBM3 in supporting influenza virus replication in the nasopharyngeal tract. Understanding IAV replication in this

environment could prove fundamental to elucidating the mechanisms of influenza transmission and reassortment.

Author Summary

To establish a productive infection, respiratory viruses must overcome or adapt to several systems within the body. One such obstacle is the temperature gradient of the respiratory tract. The upper respiratory tract, which serves as the primary route of viral transmission, provides the virus with a drastically different cellular environment compared to the lower respiratory tract, due to differences in growth temperatures. Here, we detail our investigation into the differences in the RNA binding protein (RBP) landscape between 33°C and 37°C. Our aim was to identify specific RBPs that are upregulated at 33°C and to explore their role in the influenza A virus (IAV) lifecycle, thereby advancing our knowledge of the molecular mechanisms underlying IAV infection in the upper respiratory tract. Through a combination of molecular virology and mass spectrometry, we identified a cold-inducible RBP, RBM3, as an important post-transcriptional regulator of IAV nucleoprotein (NP) mRNA. We show that RBM3 binds specifically to viral NP mRNA, stabilising the mRNA, and ultimately promoting the production of infectious virions, while abolishing the RNA binding capabilities of RBM3 reversed this effect. Overall, we find that enhanced RBM3, as seen in the upper respiratory tract, positively influences viral replication.

57 ## Introduction

58 Respiratory viruses are an ever-present pandemic concern, due in part to their airborne mode
59 of transmission [1]. While severe pathology from respiratory viruses such as influenza A virus
60 (IAV) or SARS-CoV-2 generally occurs due to viral replication in the lower respiratory tract
61 (LRT), viral transmission predominantly occurs from small droplets and aerosols from the
62 upper respiratory tract (URT) [1–4].Thus, advancing research into the unique cellular
63 environment of the nasopharyngeal epithelium is crucial to furthering our understanding of
64 viral transmission [5] and will ultimately aid public health bodies in developing the next
65 generation of nasal vaccines to boost mucosal immunity [6,7]. A key aspect of this
66 environment is the lower physiological temperature at which nasopharyngeal epithelial cells
67 grow, generally at or below 33°C, compared to the average core body temperature around
68 37°C [8]. This seemingly small difference in temperature can have wide-ranging effects on
69 normal cell biology, and by extension viral replication kinetics [9].

70 Molecular interactions and reaction kinetics are governed by thermodynamics, and
71 temperature constitutes a fundamental factor in regulating such processes. Consequently,
72 the interaction landscape, concerning both nucleic acids and proteins, is considerably
73 different in colder environments. [10]. Such variations can result in the misfolding of proteins
74 or RNA, dramatically affecting the cell as a whole [10–12]. Meanwhile, differences in affinities
75 between RNA-binding proteins (RBPs) and target RNAs can have substantial effects on an
76 array of post-transcriptional processes [13]. Although differences in transcript and protein
77 production have been observed with changing temperatures [14,15], it is not well understood
78 how, on a global level, growth temperature affects the RBPs that bind to cellular mRNAs.

79 The central aim of this study was to better understand the cellular landscape encountered by
80 respiratory viruses, with a focus on IAV, and to determine how altered growth temperature
81 affects post-transcriptional regulation of viral mRNAs. Specifically, this work investigated how
82 the overall landscape of RBPs bound to mRNAs, termed the RBPome, of lung epithelial cells
83 (A549 cells) differs between growth temperatures of 37°C and 33°C. Previous studies have
84 recently demonstrated how important the host RBPome is to viral replication, affecting
85 critical aspects of viral RNA regulation [16,17], such as nuclear export [18], translational
86 control [17] and replication [19].

87 The data presented here describes a large variation in RBPs associating with cellular mRNAs,
88 finding a comparable number of RBPs whose association with mRNA is enriched or depleted
89 at 33°C when compared to that of 37°C. One of the most interesting RBPs highlighted by this
90 study, significantly enriched in the 33C dataset, was RNA Binding Motif 3 (RBM3). This RBP is
91 a classic cold-inducible protein and is reported to be important for the management of
92 cellular stress under hypothermic conditions [20,21]. Moreover, it was recently identified by
93 ourselves and colleagues in an IAV mRNA interactome screen [22]. Here, we uncovered that
94 RBM3, through its stabilisation of viral transcripts, is wholly pro-viral during IAV infection of
95 A549 cells. Importantly, this pro-viral role was further validated in well differentiated primary
96 nasal epithelial cells (PNAECs) from multiple donors through antisense oligonucleotide (ASO)-
97 mediated overexpression of RBM3 followed by infection.

98 Overall, these findings demonstrate a vastly different regulatory landscape for RNA likely
99 exists in the human URT, where cellular growth temperatures are just a few degrees lower
100 than core body temperature. This has an important impact on the replication of respiratory
101 viruses, providing a contrasting environment to that of the lower respiratory tract, which
102 viruses must adapt to and overcome in order to transmit efficiently.

103 **Results**

104 The cold RBPome of A549 cells reveals RBM3 as a significantly enriched mRNA interactor

105 As previously mentioned, the temperature gradient normally observed in the respiratory tract
106 is known to yield distinct variations in cellular transcriptomes and proteomes [14,15] (Figure
107 1A). To identify specific RBPs that are differentially regulated through temperature, we
108 employed RNA Interactome Capture (RIC) [23] on A549 cells incubated for 48 h at 33°C or
109 37°C. This method allowed for the purification and identification of poly(A) RNA-binding RBPs
110 via UV crosslinking and mass spectrometry (Figure 1B). Quality control of the protein samples
111 to be analysed by MS was assayed by silver staining, highlighting the presence of distinct
112 protein compositions between experimental conditions (Figure 1C). We observed clear
113 differences in band patterns between the 33°C and 37°C in the pulldown samples indicative
114 of the differences between the two proteomes, which were evaluated by LC-MS/MS. The
115 resulting dataset was analysed for enrichment of RBPs in the 33°C compared to the 37°C
116 samples (Figure 1D). Adjusted P values were calculated with a cutoff of $p<0.05$. Between these
117 datasets, we identified a considerable number of RBPs that were preferentially enriched in
118 either temperature. Interestingly, a total of 209 RBPs were shared between 33°C and 37°C
119 (Figure 1E and 1F). Of the total 423 RBPs identified across all datasets, 296 were found to be
120 significantly regulated by alterations in growth temperature. Those that were present in both
121 datasets, but significantly enriched at 33°C, included RBM3, YBOX1, HNRNPC, RBM47 and
122 SND1 (Supplementary Table 1 and 2). Overall, these datasets are important evidence that the
123 RBP environment of the cell is very plastic. Several factors are selectively overrepresented at
124 cold temperatures and thus could play a role in respiratory virus infections.

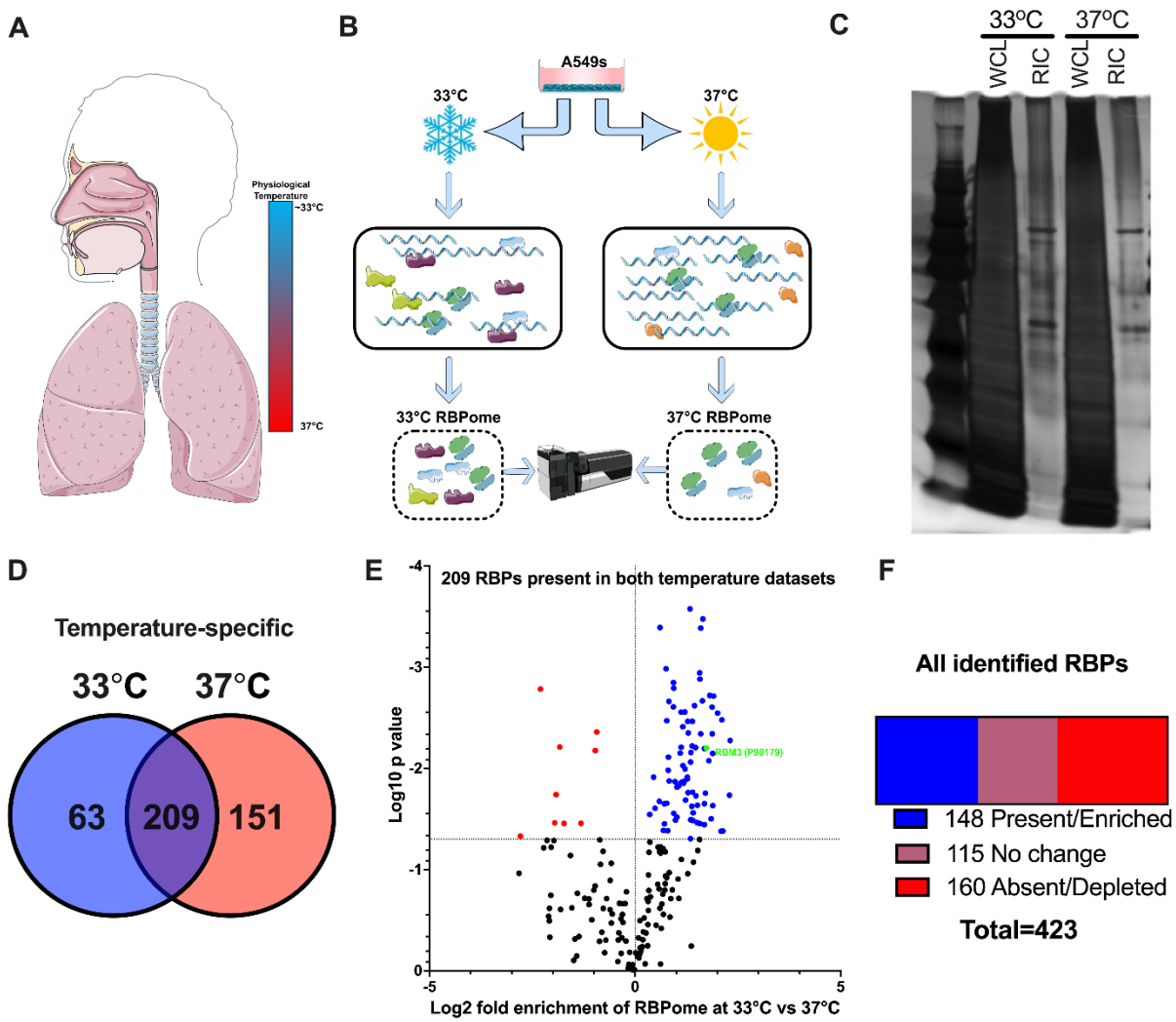

Figure 1 – Cooler growth temperatures vastly alter the RBPome of A549 cells.

***(A)** Schematic representation of the temperature gradient between the URT and LRT. **(B)** Schematic of the workflow for RIC in A549 cells incubated at 33°C or 37°C. **(C)** Representative silver stain of a gel with the RIC whole cell lysate input (WCL) and pulldown (RIC) samples from protein populations at 33°C and 37°C. **(D)** Venn diagram showing RBPs present in either 33°C datasets, 37°C datasets or both. **(E)** Volcano plot showing the enrichment of RBPs isolated from A549 33°C and 37°C pulldown samples. **(F)** Representation of the proteins significantly altered between datasets, whether by presence/absence or enrichment/depletion. Datasets derived from 3 independent biological samples.*

Loss of RBM3 negatively regulates IAV replication in A549s

One of the top hits enriched in the 33°C dataset was RBM3. This cold-inducible protein was recently identified by ourselves and our colleagues when performing an IAV A/WSN/33 NP mRNA interactome screen, and therefore presented an attractive option as an RBP that could play a role in IAV replication in the URT. Firstly, to investigate whether RBM3 impacts IAV replication we performed siRNA-mediated knockdown of RBM3 in A549 cells, followed by infection by WSN at an MOI 0.01 for 48 h. qPCR analysis confirmed effective knockdown with

140 a >95% decrease in RBM3 mRNA levels compared to a nonspecific control siRNA (NSC) (Figure
141 2A). Total RNA was harvested at 0, 8, 24 and 48 hours post infection (hpi), and levels of viral
142 mRNA were analysed via qPCR. Overall, depletion of RBM3 resulted in a significant decrease
143 in viral HA, NA, NP and M2 mRNA at 24 and 48 hpi (Figure 2B and Supp Figure 1). Most notably,
144 we observed a nearly four-fold decrease in levels of NP mRNA at 24 hpi (Figure 2B). Not
145 surprisingly, this negative impact on viral transcript levels translated through to virus
146 production, resulting in a significant drop in viral titres below the level of detection (Figure
147 2C).

148 Recently, the splicing factor Heterogenous Nuclear Ribonucleoprotein H1 (HNRNPH1), has
149 been identified to be the temperature-dependent regulator of RBM3 [13]. In brief, RBM3 pre-
150 mRNA contains exon 3a, between exons 3 and 4, whose inclusion targets RBM3 mRNA for
151 decay via the nonsense-mediated decay (NMD) pathway [24]. At 37°C HNRNPH1 binds only
152 weakly to exon 3a, resulting in the inclusion of the poison exon and a decrease in RBM3 levels.
153 However, at cooler temperatures (30-33°C), HNRNPH1 strongly binds within exon 3a,
154 resulting in the exclusion of the poison exon and a robust expression of RBM3 [13]. Here, we
155 sought to characterise the inclusion of RBM3's poison exon in A549 cells, and to assess the
156 role of HNRNPH1 as a regulator of RBM3 during IAV infection. A549 cells were transfected for
157 48 h with either siNSC or an siRNA targeting HNRNPH1 (siH1), then treated with either DMSO
158 or cycloheximide (CHX) (40 µg/mL), for 16 h. CHX treatment was used to inhibit NMD,
159 preventing the degradation of RBM3 transcripts containing the poison exon, thereby making
160 the visualisation of the poison exon easier. Total RNA was harvested 16 h post-treatment and
161 RBM3 poly(A) cDNA was generated by reverse transcription. The cDNA was PCR amplified
162 using primers spanning RBM3 exons 3 and 4, so that transcripts including exon 3a would
163 generate longer amplicons. From Figure 2D inclusion of exon 3a is clearly visible for the

164 samples that were treated with both the siHNRNPH1 and CHX, and to a much lesser extent
165 the siHNRNPH1/DMSO-treated sample. Further quantification of exon 3a inclusion by qPCR
166 showed a nearly 11-fold increase for siHNRNPH1/CHX-treated samples compared to
167 siHNRNPH1/DMSO-treated samples (Figure 2E).

168 These data confirmed that the regulation of RBM3 in A549 cells is similar to that described
169 for induced pluripotent stem cell (iPSC)-derived neurons [13]. We next investigated whether
170 knockdown of HNRNPH1 would downregulate expression of RBM3 and mirror siRBM3
171 knockdown cells. A significant decrease in RBM3 transcript levels was confirmed by qPCR
172 upon transfection with siH1 (Figure 2F). HNRNPH1-depleted A549 cells were then infected
173 with WSN (MOI 0.01), and NP mRNA transcript levels were quantified at 0, 8, 24 and 48 hpi.
174 qPCR analysis revealed a significant reduction in viral transcripts in cells transfected with siH1
175 (Figure 2G). This again translated to a significant decrease in viral titres from siH1 treated
176 cells. (Figure 2H). Taken together, abrogation of RBM3 expression, through siRNAs targeting
177 directly RBM3 or indirectly via HNRNPH1, has adverse effects on IAV replication, and may
178 affect the post-transcriptional regulation of viral mRNA.

179

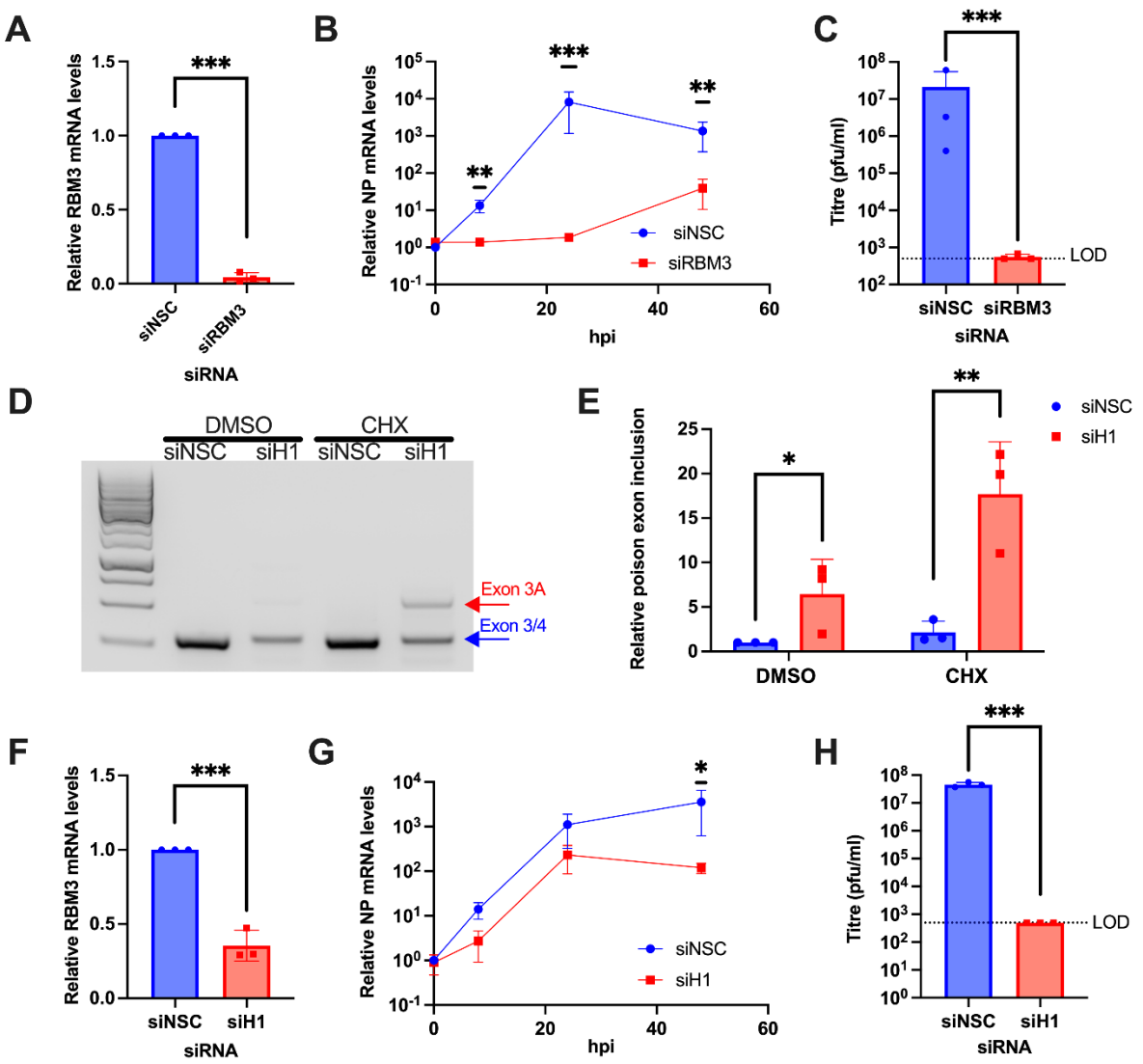

Figure 2 – Reducing RBM3 levels in A549 cells greatly inhibits IAV replication.

(A) *Quantification of RBM3 knockdown using RBM3-targeting siRNAs (siRBM3) compared to a nonspecific control siRNA (siNSC).* ***(B)*** *Transcription levels of NP mRNA in siRBM3 or siNSC treated A549 cells infected with WSN at 37°C.* ***(C)*** *Viral titres 72 hpi with WSN MOI 0.01 in siRBM3 or siNSC treated cells.* ***(D)*** *DNA gel showing inclusion of RBM3's poison exon, exon 3a. Cells were treated with siHNRNPH1 or siNSC and further treated 48 hours post-transfection with DMSO or CHX.* ***(E)*** *qPCR quantification of poison exon inclusion in the samples from Fig. 2D.* ***(F)*** *Quantification of RBM3 mRNA levels in siHNRNPH1 (siH1) A549 cells compared to siNSC treated cells.* ***(G)*** *Transcription levels of NP mRNA in siHNRNPH1 or siNSC treated A549 cells infected with WSN at 37°C. (**H**) Viral titres 72 hpi with WSN MOI 0.01 for siHNRNPH1 or siNSC treated cells.*

RBM3 overexpression increases IAV replication and binds NP mRNA

On identifying RBM3 as a potentially important RBP during IAV replication, we sought to determine whether this pro-viral phenotype arises from a direct interaction between RBM3 and viral RNA. However, as evidenced from the RIC MS, the cold environment affects the host globally, and it would be difficult to ascertain the effect of RBM3 alone on viral replication at

194 33°C. To circumvent this limitation, a cell line expressing cold-induced levels of RBM3 at 37°C
195 was needed. First, a panel of cell lines commonly used to study respiratory viruses was
196 assessed to determine their cold responsiveness, quantified by their ability to induce RBM3
197 when cultured at 33°C for 48 h. Primary nasal epithelial cells (PNECs) were used as a positive
198 control as it was expected that these would be highly responsive to cooler growth
199 temperatures. RNA was extracted and the levels of RBM3 expression were quantified by
200 qPCR, normalised to the levels observed with culturing at 37°C for each cell type (Figure 3A).
201 While PNECs were the greatest responders, with an approximate 7-fold increase in RBM3
202 mRNA levels, A549s and 293Ts both demonstrated a >3-fold increase in RBM3 levels.
203 Considering that immortalised cells can be manipulated to a greater extent that PNECs, we
204 proceeded to use A549s to develop greater mechanistic insights into the role of RBM3 during
205 IAV infection. A lentivirus-mediated stably overexpressing RBM3-Flag, clonal A549 cells line,
206 termed A549-RBM3+, was established that could be cultured at 37°C. Upon quantification by
207 qPCR, RBM3 levels were found to be >3-fold increased over an empty vector control line
208 (Figure 3B), mimicking the levels seen upon culturing of parental A549s at 33°C. Viral
209 production was then quantified in these A549-RBM3+ cells, with RBM3 overexpression
210 inducing a significant increase in viral titres of >3.5-fold (Figure 3C). Having these cell lines in
211 place, a direct interaction between RBM3 and viral transcripts could next be established.
212 Using RBPmap [25] and the published RBM3 binding motif (minimally GSNGSNG) [26], the
213 number of RBM3 high-confidence binding motifs on WSN transcripts was predicted (Figure
214 3D). While every transcript contained at least 1 putative RBM3 motif with $p<0.05$, NP mRNA
215 was predicted to have multiple highly significant binding motifs with 3 sites of $p<0.001$. These
216 data, coupled with the previously published NP mRNA interactome dataset, suggest that
217 RBM3 could directly interact with NP mRNA [22]. To confirm this hypothesis CLIP-qPCR was

218 performed in which A549-RBM3+ cells were infected at MOI 3 for 6 h, then UV crosslinked,
219 and subjected to FLAG immunoprecipitation. Finally, the covalently bound RNA was released
220 by proteinase K digestion, purified and analysed by qPCR. Flag-tagged RBM3 was efficiently
221 pulled down by an anti-Flag immunoprecipitation (Figure 3E), with Actin used as a control to
222 show that this enrichment was specific. Finally, RBM3-bound RNA was quantified by qPCR.
223 We evaluated whether NP mRNA was bound to RBM3, based on the presence of multiple
224 predicted high confidence motifs. We also quantified levels of HA mRNA as a likely non-
225 interactor and Actin mRNA as a host mRNA. We observed a strong and significant enrichment
226 of NP mRNA between the RBM3 and no primary antibody control samples, while no
227 enrichment in HA or Actin levels were observed, indicating little or no binding was by RBM3.
228 Taken together, these data indicate that an increase in RBM3 expression positively regulates
229 viral replication kinetics and establish a direct interaction between RBM3 and NP viral mRNA
230 transcripts.

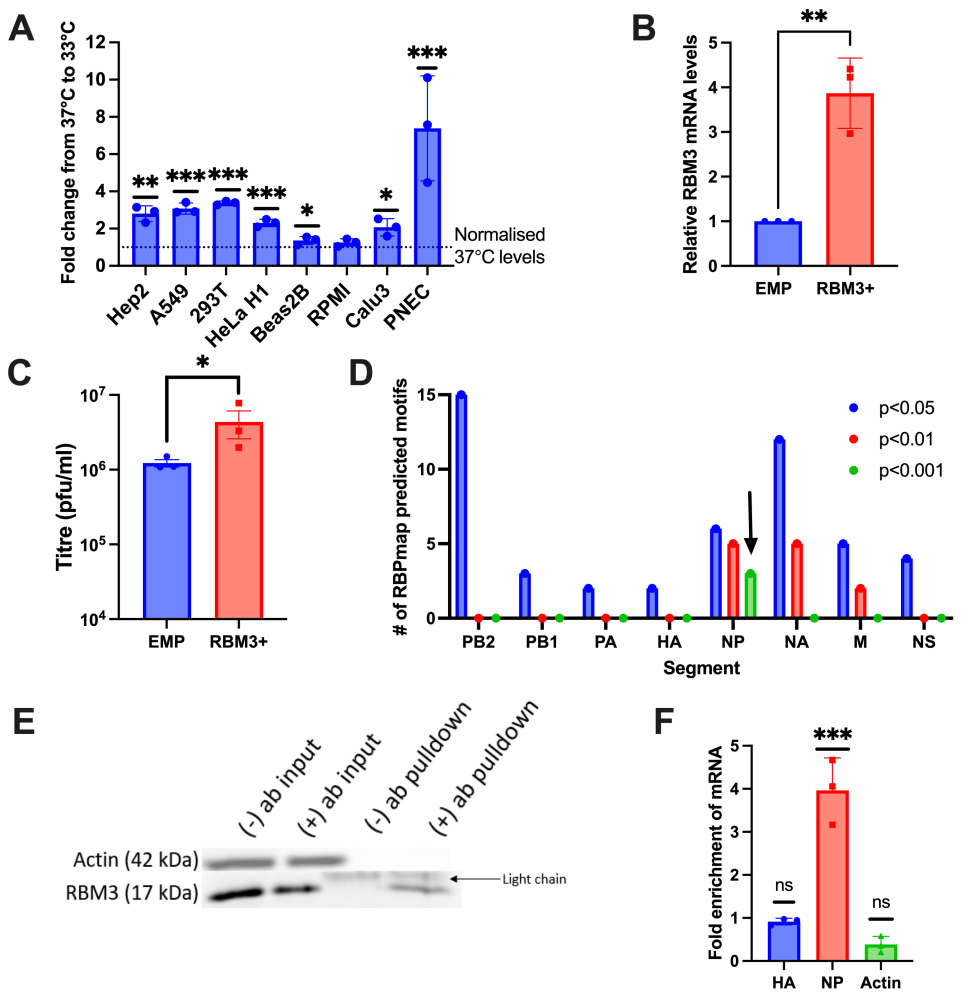

Figure 3 – RBM3 directly associates with viral transcripts, increasing overall viral replication.

(A) *Cold-responsiveness of a panel of cell lines and primary nasal epithelial cells (PNECs) as determined by the induction of RBM3 expression by qPCR over 48 h and normalised to 37°C levels.* ***(B)*** *Generation of a lentiviral RBM3 overexpression (RBM3+) A549 cell line alongside a control empty vector line (EMP).* ***(C)*** *Titres of WSN at 72 hpi after an MOI 0.01 infection in EMP or RBM3+ A549 cells.* ***(D)*** *RBPmap predicted RBM3 binding motifs for each WSN positive strand segment, separated by predicted confidence of each motif.* ***(E)*** *Western blot showing input and pulldown samples for CLIP-qPCR, blotting for Actin and overexpressed RBM3-Flag.* ***(F)*** *qPCR quantification of the RNA extracted from CLIP samples demonstrated a significant increase in viral NP mRNA levels with minimal differences in HA or Actin transcripts, when comparing RBM3 to no antibody control pulldowns.*

Overexpression of RBM3 selectively stabilises viral and cellular mRNA transcripts

Having confirmed the interaction between RBM3 and NP mRNA, we next sought to identify how this interaction positively regulates WSN replication. Previous reports have suggested that RBM3 may stabilise certain bound transcripts in neuronal cells [20,21]. Given this context, we next explored the stability of a subset of viral transcripts in the A549-RBM3+ or empty vector A549 cells. Cells were infected with WSN at an MOI 3 for 6 h, then treated with

247 actinomycin D to prevent further cellular and viral transcription [27]. Transcript levels were
248 quantified hourly over 5 timepoints from 0-4 h post-actinomycin D treatment. The data were
249 plotted to visualise the decay of RNA over this treatment period (Figure 4), with a one-phase
250 decay model fitted to the data using a least squares regression. Observed differences in RNA
251 stability were significantly different between cell lines and were assessed by comparing the
252 decay constant (k) values using an extra sum-of-squares F test, with $p<0.05$ deemed
253 significant. Although no significant effect on the stability of viral HA mRNA was observed
254 (Figure 4A), a clear and significant increase in stability was quantified for NP mRNA with a
255 >70% increase in RNA half-life (Figure 4B). While viral M2 mRNA showed a modest increase
256 in half-life but no significant difference in stability (Figure 4C), it is noteworthy that
257 overexpression of RBM3 significantly and positively regulated cellular GAPDH levels (Figure
258 4D). This suggests that RBM3 stabilises mRNA transcripts, likely a form of cellular post-
259 transcriptional regulation for transcripts such as GAPDH, YAP1 [20] or GAS6 [21]. This
260 mechanism is seemingly exploited by IAV during infection to promote viral transcript stability
261 and overall viral replication.

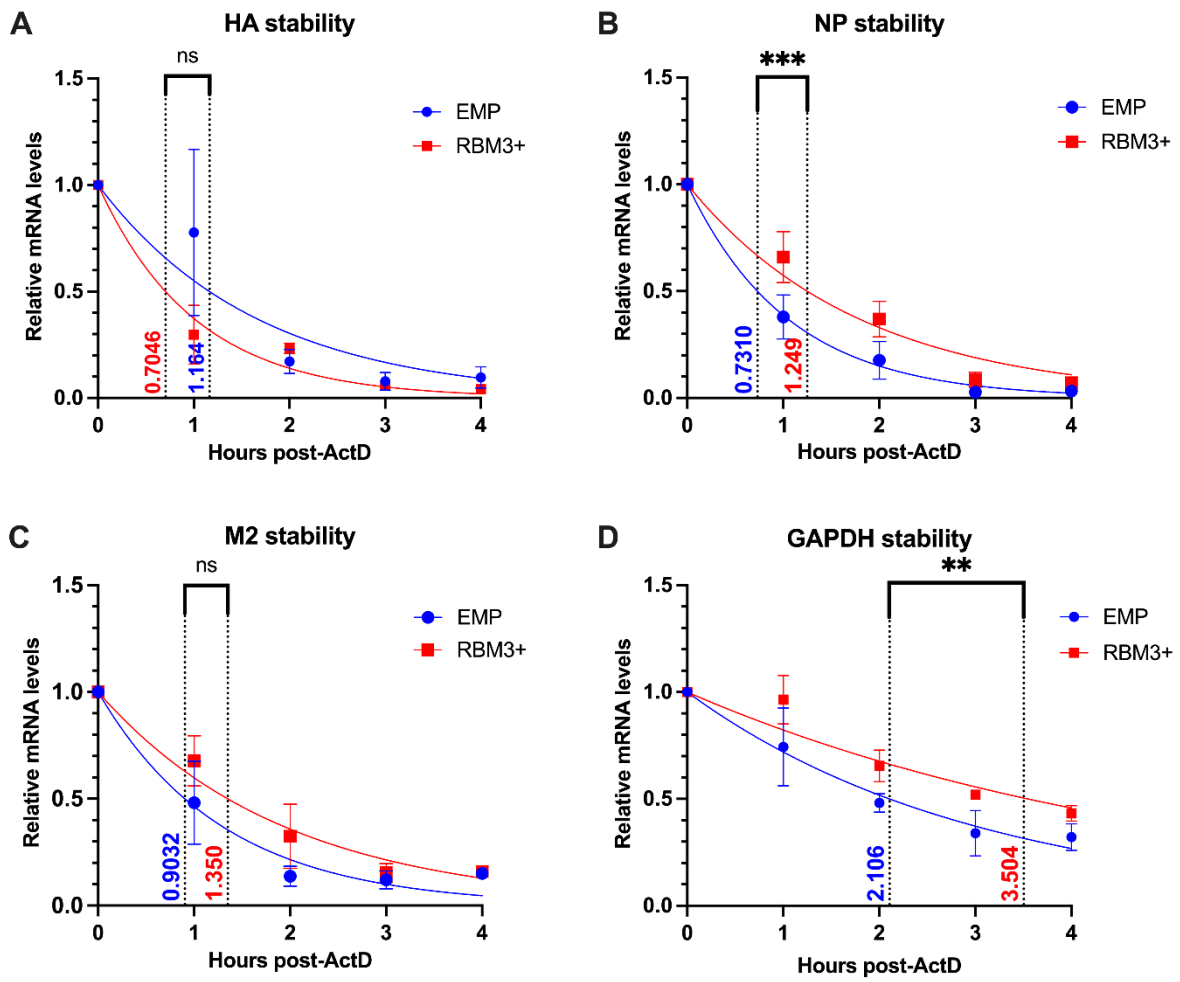

262

263 *Figure 4 – Binding of RBM3 has a stabilising effect on mRNA transcripts.*

264 *Transcript stability in empty vector or RBM3 overexpression A549 cells was established by an actinomycin D (ActD) assay*
265 *commenced at 6 hpi. Viral transcripts HA **(A)**, NP **(B)** and M2 **(C)**, and the cellular transcript GAPDH **(D)** were quantified over*
266 *5 hours with transcript half-lives quantified by a one-phase decay using a least squares regression.*

267 <u>An RNA-binding null RBM3 confirms the stabilisation of RBM3-bound transcripts</u>

268 RBM3 is composed of two major domains; an RNA Recognition Motif (RRM) found at the C-
269 terminus, and an N-terminus arginine-glycine rich (RGG) domain (Figure 5A) [28]. The former
270 contains two highly conserved RNA binding regions, RNP2 and RNP1. After establishing the
271 binding between NP mRNA and RBM3, we proceeded to investigate how an RNA-binding null
272 mutant RBM3 would affect viral replication. We hypothesised that any pro-viral function
273 would be lost through ablation of RNA-binding. To test this, we created an RBM3 RNA-binding
274 null mutant cell-line, in which mutations were introduced to substitute phenylalanine (F)

residues within RNP2 and RNP1 to leucine (L) (Figure 5A). Previous studies have shown that single L>F substitutions within RNP motifs disrupt the RNA binding ability [29]. When viral titres from infected A549-RBM3+ and A549-RBM3 mutant cell lines were compared (Figure 5B), we observed a significant >95% decrease in titres from the RBM3 mutant cells. Actinomycin D assays to determine RNA stability were repeated in A549-RBM3+ and RBM3 mutant cell lines. These revealed a loss of the stabilisation phenotype in the RBM3 mutant cells for viral NP transcripts as well as cellular GAPDH (Figure 5C and 5D). Interestingly, a 70% decrease in half-life for NP mRNA in the RBM3 mutant cells was observed, mimicking the phenotype observed in the A549-EMP cells. These results indicate that, through mutation of the RNA-binding motifs of RBM3 to generate an RNA-binding null mutant, we can obviate the stabilisation capacity of RBM3, consequently leading to a decrease in virus output.

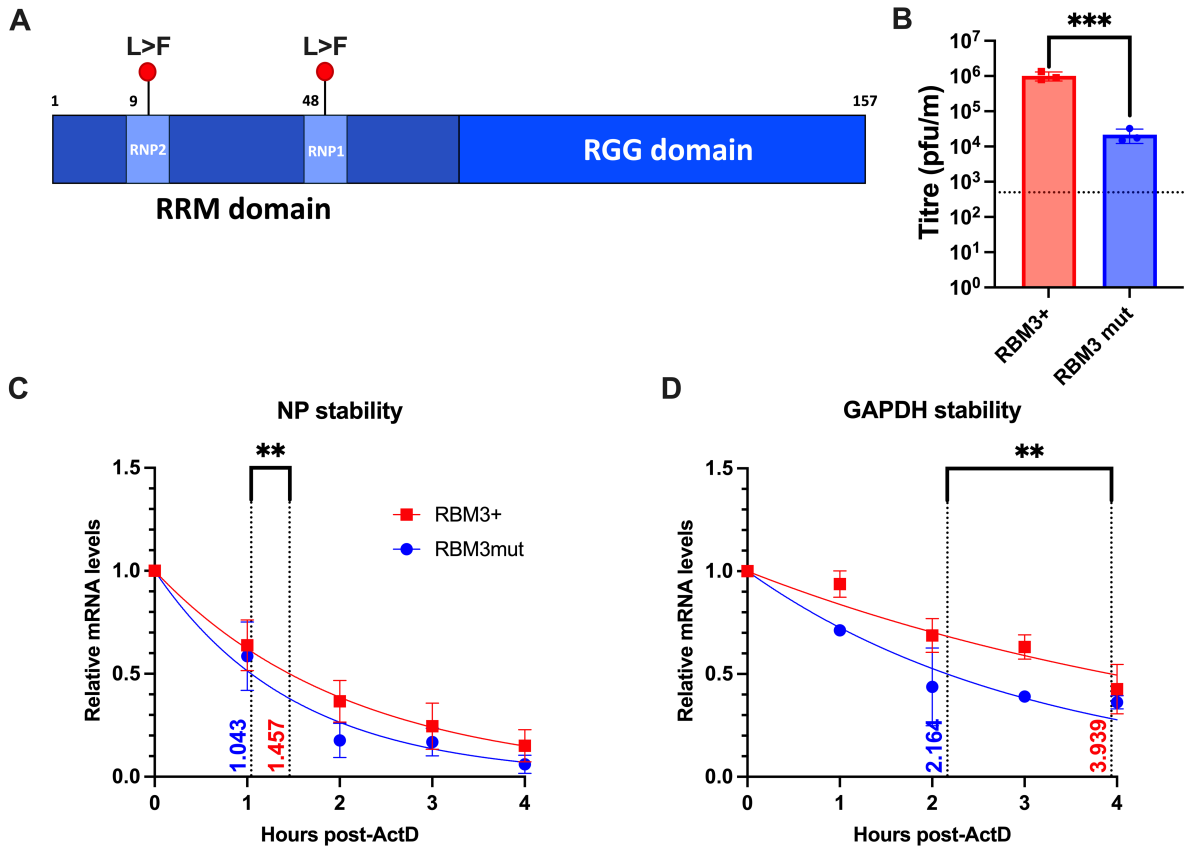

Figure 5 – Stability of mRNAs conferred by the overexpression of RBM3 is lost upon mutagenesis of the RNA-binding domains.

288 ***(A)*** *Schematic representation of RBM3. Single nonsense mutations were introduced into the RNA binding domains, RNP2 and*
289 *RNP1, creating an RNA-binding null mutant RBM3.* ***(B)*** *A549-RBM3+ or A549-RBM3 mut cells were infected at MOI 0.01 with*
290 *WSN for 48 hours. Supernatants were harvested and titrated. Dotted line indicates the limit of detection.* ***(C,D)*** *A549-RBM3+*
291 *or A549-RBM3 mut cells were infected with MOI 3 WSN for 6 hours, then treated with ActD. Viral NP transcripts (C) and*
292 *cellular GAPDH (D) were quantified over 4 hours with transcript half-lives quantified by a one-phase decay using a least*
293 *squares regression.*

294 ASO-mediated increase of RBM3 levels in primary cells promotes overall viral replication

295 Finally, we wanted to determine whether RBM3-mediated increase of overall viral replication
296 would be mirrored in PNECs. Previous studies have determined that targeted ASO treatment
297 of the RBM3 poison exon Ex3a in immortalised cell lines can result in the exclusion of the
298 poison exon, preventing NMD of RBM3 transcripts, and thus increasing overall RBM3 levels,
299 effectively mimicking the function of HNRNPH1 [24]. Treatment of A549 cells with this
300 previously published Ex3a-specific ASO for 48 h resulted in an almost 4-fold increase in RBM3
301 transcript levels compared to that of a non-targeting control (Figure 6A), confirming its
302 effectiveness. Next, ASO treatment was applied apically to PNEC cultures from 3 donors.
303 Primary cells are much less permissive to transfection, therefore, ASO treatment would be
304 predicted to be much less effective at inducing RBM3 in these cultures. Nevertheless, we
305 observed a robust and significant ~50% increase in RBM3 transcript levels after 48 h
306 compared to the control ASO for all 3 donors (Figure 6B). Following this, we subjected PNEC
307 cultures from the same 3 donors to ASO treatment followed by infection with WSN for 48 h.
308 We then evaluated viral replication in these PNECS by quantification of viral RNA levels at 48
309 hpi. A significant increase in both NP mRNA and vRNA levels was observed by qPCR for each
310 donor upon treatment with the Ex3A-specific ASO, with mRNA levels on average more than
311 doubling after Ex3a ASO treatment (Figure 6C). These data confirm our earlier observations
312 that increasing RBM3 levels positively regulates IAV replication, in a highly relevant human
313 respiratory epithelial model of infection.

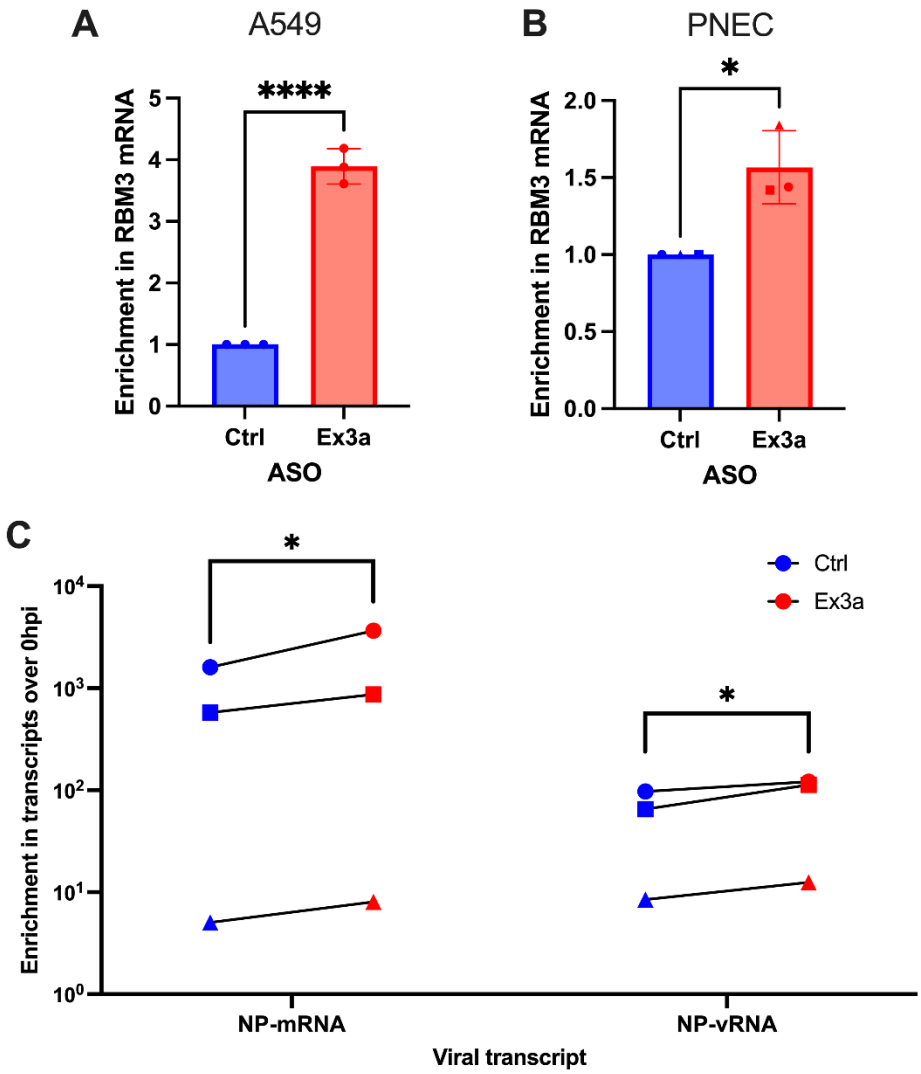

314

315 *Figure 6 - Increasing expression of RBM3 in PNECs significantly increases IAV replication*

316 ***(A)*** *Control (Ctrl) or Exon3a (Ex3a) specific ASOs were initially tested in A549 cells to determine their effectiveness in increasing*
317 *overall RBM3 mRNA levels, with an approximate 4-fold increase observed at 48 h post-transfection.* ***(B)*** *This was replicated*
318 *in PNECs at 48 h post-transfection where an approximate 50% ASO-mediated increase in RBM3 levels was quantified.* ***(C)***
319 *Quantifying viral mRNA and vRNA production in 3 donors (indicated by different shaped data points) previously treated with*
320 *Ctrl or Ex3a ASOs, demonstrated a significant increase in overall viral replication at 48 hpi.*

321

322 ## Discussion

323 Considering the persistent threat of a respiratory virus pandemic, whether that be another
324 coronavirus as seen with SARS-CoV-2, or a novel influenza strain such as the avian H5N1
325 circulating globally in wildlife, a thorough understanding of the tissues in which these viruses
326 replicate is critical to combat potential pandemic risk. The URT serves as an important tissue
327 for understanding the transmission of these respiratory virus. To prevent onward
328 transmission, it is critical to limit viral replication and shedding from the URT [7]. Therefore,
329 there is a need to better characterise the cell biology of the URT, specifically the
330 nasopharyngeal epithelium, to uncover unique virus-host interactions that may be essential
331 for viral replication. Given the nasopharyngeal tissue of the URT is cooler than conventional
332 core body temperature of around 37°C, it is likely that this reduction in temperature will have
333 substantial effects on cell biology, resulting in important mechanistic differences in viral
334 replication.

335 Herein, we uncovered how the overall environment of mRNA-binding proteins is altered in
336 A549 cells cultured at 33°C compared to 37°C, and investigated how this would affect IAV
337 replication. While we identified 63 RBPs unique to our 33°C dataset and 151 unique to our
338 37°C dataset, there were 209 RBPs in common between both growth temperatures. RBM3
339 was one such factor, shown to be significantly enriched on mRNAs at 33°C compared to 37°C.
340 RBM3 is a known cold-inducible protein that has recently been shown to be regulated by the
341 binding efficiency of HNRNPH1 to a poison exon [13]. Studies have uncovered a role for RBM3
342 in promoting cell survival during cold stress [30,31], which may be due to positive regulation
343 of post-transcriptional processes including mRNA stability [20,21] and translation [32]. Aside
344 from RBM3, several of the most enriched RBPs we observed in the 33°C RBPome, including

345 SND1, HNRNPC, TIA1 and ZC3H11A, have previously been reported to directly associate with
346 and regulate the RNAs of multiple respiratory viruses. SND1 has been reported to associate
347 with SARS-CoV-2 negative-sense RNA, with its binding required for viral RNA synthesis [19].
348 HNRNPC and TIA1 have also been identified as important SARS-CoV-2 RNA binders, both
349 promoting overall virus replication [33,34]. Additionally, ZC3H11A has been shown to
350 positively regulate polyadenylation of HAdV-5 viral transcripts [35] and a further cold-
351 enriched RBP, YBOX1, may direct IAV vRNPs to the microtubule organising centre (MTOC)
352 [36].

353 Furthermore, RBM47 was found to be enriched over 3.5-fold in the 33°C dataset over that of
354 the 37°C. RBM47 is a broadly anti-viral RBP that has been shown to increase in expression in
355 the presence of viral infection or IFN stimulation and is essential for enhancing host IFN
356 signalling [37]. Given that we have identified a greater level of RBM47 on cellular mRNAs at
357 33°C, it is interesting to speculate what role this may play in the baseline innate immune
358 responses of nasopharyngeal epithelial cells. If the increased abundance of RBM47 on host
359 mRNAs leads to a more anti-viral environment through enhancement of IFN signalling, then
360 RBM47 may be an important factor for our understanding of viral replication kinetics in the
361 URT and warrants further investigation.

362 With strong evidence that RBM3 is highly expressed in the URT [38], positively regulates
363 bound RNAs [20,21], and may bind to IAV NP mRNAs [22], we investigated how RBM3 directly
364 affects IAV replication. Knockdown of RBM3 resulted in a significant reduction in viral tires
365 and mRNA production. However, this is not necessarily indicative of a direct interaction
366 between RBM3 and viral mRNAs. Through a combination of RBPmap prediction [25] of RBM3
367 binding motifs within WSN transcripts and CLIP-qPCR, we confirmed that RBM3 directly
368 interacts with at least the NP mRNA of WSN. We next investigated how NP mRNA may be

369 affected by RBM3 binding. Recent studies identified RBM3 as a likely stabilising factor for
370 YAP1 [20] and GAS6 [21] transcripts, thus we investigated the stability of viral mRNAs in our
371 RBM3 overexpressing A549 cell line. We observed a significantly elongated degradation
372 profile for NP mRNA when RBM3 was overexpressed, but this was lost upon mutagenesis of
373 the RNA-binding domains of RBM3. Finally, to validate whether this phenotype translates to
374 a more clinically relevant model of IAV infection, we used a targeted ASO treatment to
375 increase RBM3 expression in primary nasal epithelial cells, prior to infection. While there was
376 the expected donor-to-donor variability in infection levels, overall higher levels of RBM3
377 expression in each donor had a significant effect on multicycle viral replication, quantified by
378 increases in both NP mRNA and vRNA levels.

379 From these data, it is clear that the increased levels of RBM3 found in the nasopharyngeal
380 tissue of the URT would provide a pro-viral environment for IAV replication and transmission.
381 However, it remains to be determined if this would extend to the positive regulation of other
382 respiratory viruses. We have shown that RBM3 directly binds to IAV transcripts, with a
383 particular focus on NP mRNA. As RBM3 clearly increases the stability of NP mRNA, it is
384 incumbent to further investigate how cooler temperatures affect more general aspects of
385 RNA biology. Some cellular processes slow down due to cooler growth temperatures, with
386 translation rates being a key process among those reported to measurably decline [32].
387 Consequently, mature mRNAs would have to reside in the cell longer to be efficiently
388 translated. It is worth speculating that the stabilising role for RBM3 may then be in directly
389 preventing bound mRNAs from degradation by nucleases. This may be through protecting the
390 bound mRNA from endonuclease recognition and cleavage, or inhibiting binding of decay
391 factors, such as the exosome complex [39]. Alternatively, Dresios et al., have reported that
392 overexpression of RBM3 enhances protein synthesis of targeted genes [32]. As stated earlier,

393 it is well known that cooler growth conditions inhibit protein synthesis. Therefore, if RBM3
394 increases the ribosome loading of bound transcripts, the protection conferred by the
395 translation machinery would positively regulate transcript half-life. However, it cannot be
396 discounted that stability stemming from RBM3 binding may arise from stabilisation of RNA
397 secondary structures shown to be important for viral RNAs [40], modulation of RNA
398 modifications which are known to affect IAV transcripts [41], or even sequestration of mRNA
399 into membraneless organelles, already known to be important during vRNA trafficking [42].
400 While it appears IAV has evolved to recruit RBM3 to NP mRNA to positively regulate transcript
401 stability, and by extension overall IAV replication, we should also consider that this
402 mechanism of action may be hijacked for therapeutic purposes. With the seemingly rapid,
403 and successful deployment of mRNA vaccines to combat severe pathology arising from a
404 pandemic respiratory virus [43], in SARS-CoV-2, the next potential avenue in pandemic
405 preparedness would be the development of nasal vaccines that can induce a robust IgA
406 response and prevent onward transmission from the URT [44,45]. With an inhalable form of
407 mRNA therapeutic having recently been successfully delivered to the airways of mice [6], it is
408 perhaps pertinent to explore whether the mRNA stabilising effects of RBM3 may be exploited
409 to enhance such therapies in the future.
410 Herein, we present RBM3 as an important host factor for IAV replication in the URT. RBM3 is
411 highly expressed in the nasopharyngeal tract due to cooler growth temperatures influenced
412 by the external environment. RBM3 binds to and stabilises IAV NP mRNA, while its loss has a
413 significantly inhibitory effect on viral replication. Taken together, it is clear that RBM3 is an
414 important host factor for efficient replication and onward transmission of IAV from the
415 nasopharyngeal tract.

416 **Methods**

417 Cells

418 All immortalised cell lines were cultured in DMEM supplemented with 1% Pen-Strep (Thermo
419 Fisher Scientific; 15140122) and 5% FBS (Thermo Fisher Scientific; 10270106) at 37°C/33°C
420 and 5% CO_2. Cell lines used were A549s (ATCC; CCL-185), HEK 293Ts (ATCC; CRL-3216), MDCKs
421 (CCL-34), Hep2s (ATCC; CCL-23), HeLa H1s (ATCC; CRL-1958), Beas2Bs (ATCC; CRL-3588), RPMI
422 2650s (ATCC; CCL-30) and Calu3s (ATCC; HTB-55).

423 Virus stocks and infections

424 IAV WSN (A/WSN/33) stocks were generated from a reverse genetics system previously
425 described [46]. WSN stocks were grown on MDCK cells in IAV growth media consisting of
426 DMEM, Pen-Strep, 0.2% BSA (Merck; A8412), 25mM HEPES (Merck; H0887) and TPCK-trypsin
427 (Merck; T8802) and titrated on MDCK cells by plaque assay.

428 RIC

429 The protocol employed here to capture the RNA interactome of poly(A)+ RNA (RIC) from A549
430 cells has been described previously [17,23]. However, we made one minor modification. At
431 the time of seeding, 48 h before crosslinking and harvesting, A549 cells were either incubated
432 under the normal growth temperature of 37°C, to determine the 37°C RBPome, or incubated
433 in a 33°C incubator, to determine the 33°C RBPome. Cells were grown for 48 h at these
434 conditions before performing UV crosslinking at 254nm and lysis. The remaining steps were
435 followed exactly as has been described previously [23].

436 Protein visualisation

437 Western blotting was performed as has been previously described [47]. Primary antibodies
438 for influenza PA (Thermo Fisher Scientific; Pa5-32223), RBM3 (Proteintech; 14363-1-AP),
439 ACTB (Proteintech; 66009-1-ig), and Flag (Proteintech; 66008-3-ig) were all used at a 1:5000
440 dilution. Proteins bands on blots were visualised by chemiluminescence. Total protein was
441 imaged by silver staining (Thermo Fisher Scientific; 24612), following the manufacturer's
442 protocol.

443 LC-MS/MS and data analysis

444 Mass spectrometry of RIC samples was performed at the Cambridge Centre for Proteomics.
445 Sample treatment, preparation and trypsin digestion were performed as described previously
446 [48]. Data for each sample were acquired on an Orbitrap Fusion Lumos Tribrid mass
447 spectrometer over a 60 min run. No fractionation was performed due to the likely low
448 complexity of the sample. Raw mass spectrometry data was analysed using MaxQuant
449 software (v2.4.7.0) and utilising the Andromeda search engine [49]. The MS/MS spectra were
450 aligned to the Uniprot Homo sapiens protein database, with known mass spectrometry
451 contaminants and reversed sequences also included. The search was performed with trypsin
452 selected as the specific enzyme and a maximum of 2 missed cleavage events allowed. The MS
453 accuracy was set to 10 ppm, then 0.05 Da for the MS/MS. The maximum peptide charge was
454 set to seven and seven amino acids were required for the minimum peptide length. One
455 unique peptide to the protein group was required to call the presence of a specific protein,
456 while a false-discovery rate (FDR) of 1% was set. Statistical analysis to determine enriched
457 proteins in one set of biological samples over another was performed using the intensities
458 quantified by MaxQuant on Perseus software (v2.0.11) [50]. First, any potential contaminants,
459 reverse hits or proteins that were not well identified (fell below 1% FDR) were removed. Then

460 only proteins that were identified in at least 2 replicates from a single biological condition
461 were utilised. After filtering, the intensities were log transformed (log_2) and statistical
462 significance was calculated by way of an unpaired two-tailed Student's t-test for each protein
463 group. These values were then log transformed ($-log_{10}$) and the resulting p values and
464 enrichments were graphed as volcano plots. The cutoff for statistical significance was set to
465 $p < 0.05$.

466 siRNA knockdowns

467 A pair of siRNAs targeting the specified mRNA were used in each knockdown experiment,
468 aside from when a single non-specific control siRNA (siNSC) was used. Sequences of these
469 siRNAs are listed in Supplementary Table 3. A final concentration of 20nM total siRNA was
470 used, and these were transfected using Lipofectamine RNAiMAX (Invitrogen; 13778075)
471 following the manufacturer's instructions. A549 cells were seeded and transfected
472 simultaneously and incubated for 24 h, after which media was changed with fresh growth
473 media. Cells were then incubated for a further 24 h prior to infection.

474 Establishment of a RBM3 overexpression cell line using a lentiviral vector

475 A lentiviral expression plasmid was generated encoding for either a full length wild-type RBM3
476 C-terminally tagged with 2X Flag epitope tags (RBM3+), a full-length RNA-binding mutant
477 (RBM3-Mut), containing two single phenylalanine to leucine substitutions within RNP1 (L48F)
478 and RNP2 (L9F), or an empty vector (A549-EMP). A549-RBM3, A549-EMP and A549-Mut were
479 followed by a P2A self-cleaving peptide and a puromycin resistance gene, similar to a system
480 we have published previously [41]. Again, similar to previous publications, we rescued
481 lentiviral particles by co-transfecting 293T cells with the RBM3, RBM3 Mut or EMP lentiviral
482 vector alongside d8.74 (Addgene; 22036) and MD2G (Addgene; 12259). At 72 h post-

483 transfection the supernatant was harvested, passed through a 0.45 μm filter and then
484 overlaid onto fresh A549 cells. At 72 h post transduction cells were treated with 2 μg/ml
485 puromycin and left to select for 72 h. Cells were then single cell cloned in 96 well plates in the
486 presence of 2 μg/ml puromycin and left to grow for 3 weeks. Single cell colonies were then
487 selected, expanded, and checked by Western blot to confirm the expression of the transgene.

488 CLIP-qPCR

489 The CLIP-qPCR protocol employed here has been published previously [51]. Briefly, A549-
490 RBM3 and A549-EMP cells were seeded one day prior to infection. Cells were infected with
491 A/WSN/33 at an MOI 3 PFU/cell and incubated for 6 h. At 6 hpi media was removed from the
492 cells, before being washed in ice cold PBS. UV crosslinking was performed at 254nm. Cells
493 were then scraped, pelleted and lysed in 250 µl of NP40 lysis buffer (HEPES-KOH pH 7.5
494 50mM, KCl 150mM, EDTA pH 8.0 2mM, NaF 1mM and NP40 0.5%) on ice for 30 min. Lysates
495 were clarified by centrifugation and 10% of the sample was saved as an input and boiled in
496 Laemmli buffer containing 2% β-mercaptoethanol at 95°C for 10 min for western blotting. The
497 remaining 90% of lysate underwent immunoprecipitation with anti-Flag antibody (Merck,
498 F1804) coupled to Protein G Dynabeads (ThermoFisher, 10004D) for 1 h at room temperature.
499 Beads were then captured, washed five times with 1 mL NP40 lysis buffer and three times
500 with PBS. A fraction (10%) of the beads was removed, resuspended in Laemmli buffer and
501 boiled at 95°C for 10 min for Western blotting. The remaining 90% of beads underwent
502 proteinase K digestion (ThermoFisher, EO0491) at 55°C for 60 min to release bound RNA,
503 following the manufacturer's instructions. RNA was then isolated from the digestion by TRIzol
504 LS (ThermoFisher, 10296028) and ethanol precipitation and cDNA were synthesized using
505 oligo dT or A/WSN/33 specific primers [52] (Supplementary Table 4). Quantification of the

506 cDNAs was performed by qPCR, as described below. Fold enrichment of RNA levels was
507 quantified using the ΔΔCT method and normalised to input levels.

508 IAV growth kinetics at 37°C and 33°C

509 For multicycle IAV infections, A549 cells were seeded 48hrs before infection. Cells were
510 infected with A/WSN/33 at an MOI 0.01 PFU/cell in DMEM for 1 h. The inoculum was then
511 removed, and cells incubated for 48 h in IAV growth media, described above, supplemented
512 with TPCK-trypsin. Supernatants were then titrated on MDCK cells by plaque assay.

513 IAV qPCR growth curves

514 A549 cells were infected with A/WSN/33 virus at an MOI 0.01 PFU/cell. At 0, 8, 24 and 48 hpi
515 RNA was extracted from cells using TRIzol (Invitrogen; 15596026). RNA was isolated and
516 precipitated following the manufacturer's instructions and 200ng was reverse transcribed
517 into cDNA using the ABI cDNA synthesis kit (Applied Biosystems; 4368814). For all cellular
518 targets RT was performed using an oligo dT, while viral RNA underwent separate RT reactions
519 with primers specific to each mRNA or vRNA [52]. These primers are listed in Supplementary
520 Table 4 alongside the primers used for qPCR amplification. All qPCR experiments were
521 performed using SYBR Select Master Mix (Applied Biosystems; 4472908) following the
522 manufacturer's instructions. All qPCR data were quantified using the ΔΔCT method.

523 Actinomycin D assays

524 A549-RBM3+, A549-Mut and A549-EMP cells were seeded at a density of 1 x 10^5 cells/well
525 one day prior to infection. Cells were infected with WSN at a MOI of 3 PFU/cell. At 6 hpi, RNA
526 was harvested from a single well for each cell type, constituting the 0 h timepoint. All
527 remaining infected wells underwent media exchange for growth media containing containing
528 2 µg/mL Actinomycin D (SBR00013). RNA was harvested hourly from 7-10 hpi representing 1-

529 4 h post Actinomycin D treatment. RNA underwent cDNA conversion using oligo dT or
530 A/WSN/33 specific primers, with the ABI cDNA synthesis kit (Applied Biosystems; 4368814).
531 Quantification of the cDNAs was performed by qPCR, described above. Fold enrichment of
532 RNA levels was quantified using the ΔΔCT method and normalised to either A549-EMP or
533 A549-RBM3 levels.

534 Well-Differentiated Primary Airway Epithelial Cell Culture

535 Primary nasal epithelial cells were obtained from Promocell and well differentiated primary
536 nasal epithelial cell (WD-PNEC) cultures were established as described previously [53]. Briefly,
537 WD-PNECs were seeded onto collagen coated 6 mm Transwells (Sarstedt, 83.3932.041) at
538 $3x10^4$ cells/transwell. Cells were submerged in modified Promocell Airway Epithelial Cell
539 Growth Medium which was replaced on the apical and basal side every 2 days until the cells
540 reached confluency. Once confluent, an air liquid interface (ALI) was initiated by completely
541 removing the apical medium. Cells were differentiated using Pneumacult ALI medium
542 (Stemcell Technologies, #05001) supplemented with hydrocortisone and heparin. For
543 downstream experiments, WD-PNECs were only used when there was extensive cilia
544 coverage and mucus production, clear hallmarks of full differentiation.

545 ASO transfection and IAV infection of cells

546 A549s were transfected with control or Exon 3a targeting ASOs [24] (Supplementary Table 5)
547 to initially test whether induction of RBM3 could be achieved in airway cells. ASOs were
548 resuspended in DMEM at a concentration of 1 µM and transfected using Lipofectamine 2000
549 (Invitrogen, 1 µL/mL). At 48 h post-transfection RNA was harvested, cDNA synthesised as
550 described above, and RBM3 levels quantified by qPCR. For WD-PNEC cells, the transfection

551 conditions were the same, with the ASO-containing transfection mix added apically to WD-
552 PNECs. Cells were incubated for 48 h prior to infection with WSN MOI 0.01 PFU/cell in DMEM.
553 At 1 hpi, the inoculum was removed and transwells were washed 5 times in DMEM to remove
554 unbound virus. RNA was harvested from WD-PNECS using Trizol™ either before infection or
555 at 72 hours post-infection.

556 Statistical analysis

557 Unless otherwise stated, all experiments were performed as 3 independent biological
558 replicates. When bar graphs are used to represent the data, each individual replicate can be
559 observed as a point overlaid on the bar, with error bars indicating standard deviation.
560 Significance was calculated by performing Student's t-test with * indicating $p<0.05$, **
561 indicating $p<0.01$ and *** indicating $p<0.001$.

562

563 **Acknowledgements**

564 This research was funded in part by an ERC-STG grant, PTFLU 949506 awarded to D.G.C. This
565 research received infrastructure support from the Wellcome-Wolfson Institute for
566 Experimental Medicine at Queen's University Belfast.

567 In Figure 1 cells_bilayer icon by Marcel Tisch is licensed under CC0, upper-respiratory-tract
568 icon by Servier https://smart.servier.com/ is licensed under CC-BY 3.0 Unported, lung icon by
569 Servier https://smart.servier.com/ is licensed under CC-BY 3.0 Unported, all protein icons by
570 Servier https://smart.servier.com/ is licensed under CC-BY 3.0 Unported,
571 Liquid_Chromatograph_Mass_Spectrometer icon by DBCLS

https://togotv.dbcls.jp/en/pics.html is licensed under CC-BY 4.0 Unported and rna icon by Servier https://smart.servier.com/ is licensed under CC-BY 3.0 Unported.

575 ## References

576 1. Lakdawala SS, Jayaraman A, Halpin RA, Lamirande EW, Shih AR, Stockwell TB, et al.
577 The soft palate is an important site of adaptation for transmissible influenza viruses.
578 Nature. 2015;526: 122–125. doi:10.1038/nature15379

579 2. Xie C, Su W, Sia SF, Choy KT, Morrell S, Zhou J, et al. A(H1N1)pdm09 Influenza Viruses
580 Replicating in Ferret Upper or Lower Respiratory Tract Differed in Onward
581 Transmission Potential by Air. J Infect Dis. 2022;225: 65–74.
582 doi:10.1093/INFDIS/JIAB286

583 3. Richard M, van den Brand JMA, Bestebroer TM, Lexmond P, de Meulder D, Fouchier
584 RAM, et al. Influenza A viruses are transmitted via the air from the nasal respiratory
585 epithelium of ferrets. Nature Communications 2020 11:1. 2020;11: 1–11.
586 doi:10.1038/s41467-020-14626-0

587 4. Varble A, Albrecht RA, Backes S, Crumiller M, Bouvier NM, Sachs D, et al. Influenza A
588 Virus Transmission Bottlenecks Are Defined by Infection Route and Recipient Host.
589 Cell Host Microbe. 2014;16: 691–700. doi:10.1016/J.CHOM.2014.09.020

590 5. Bisht K, te Velthuis AJW. Decoding the Role of Temperature in RNA Virus Infections.
591 mBio. 2022;13.

592 6. Suberi A, Grun MK, Mao T, Israelow B, Reschke M, Grundler J, et al. Polymer
593 nanoparticles deliver mRNA to the lung for mucosal vaccination. Sci Transl Med.
594 2023;15.

595 7. McMahan K, Wegmann F, Aid M, Sciacca M, Liu J, Hachmann NP, et al. Mucosal
596 boosting enhances vaccine protection against SARS-CoV-2 in macaques. Nature 2023
597 626:7998. 2023;626: 385–391. doi:10.1038/s41586-023-06951-3

598 8. Eccles R. Why is temperature sensitivity important for the success of common
599 respiratory viruses? Rev Med Virol. 2021;31: 1–8. doi:10.1002/RMV.2153
600 9. Otter CJ, Fausto A, Tan LH, Khosla AS, Cohen NA, Weiss SR. Infection of primary nasal
601 epithelial cells differentiates among lethal and seasonal human coronaviruses. Proc
602 Natl Acad Sci U S A. 2023;120: e2218083120.
603 doi:10.1073/PNAS.2218083120/SUPPL_FILE/PNAS.2218083120.SAPP.PDF
604 10. Pullara P, Alshareedah I, Banerjee PR. Temperature-dependent reentrant
605 phase transition of RNA-polycation mixtures. Soft Matter. 2022;18: 1342–1349.
606 doi:10.1039/D1SM01557E
607 11. Riback JA, Katanski CD, Kear-Scott JL, Pilipenko E V., Rojek AE, Sosnick TR, et al.
608 Stress-Triggered Phase Separation Is an Adaptive, Evolutionarily Tuned Response.
609 Cell. 2017;168: 1028-1040.e19. doi:10.1016/J.CELL.2017.02.027
610 12. Tauber D, Tauber G, Parker R. Mechanisms and Regulation of RNA
611 Condensation in RNP Granule Formation. Trends Biochem Sci. 2020;45: 764–778.
612 doi:10.1016/J.TIBS.2020.05.002
613 13. Lin JQ, Khuperkar D, Pavlou S, Makarchuk S, Patikas N, Lee FC, et al. HNRNPH1
614 regulates the neuroprotective cold-shock protein RBM3 expression through poison
615 exon exclusion. EMBO J. 2023;42: e113168. doi:10.15252/EMBJ.2022113168
616 14. Cugusi S, Mitter R, Kelly GP, Walker J, Han Z, Pisano P, et al. Heat shock induces
617 premature transcript termination and reconfigures the human transcriptome. Mol
618 Cell. 2022;82: 1573-1588.e10.
619 doi:10.1016/J.MOLCEL.2022.01.007/ATTACHMENT/F4235ADB-517D-41B2-B14B-
620 196321576620/MMC5

621 15. Gagnon D, Barry H, Barhdadi A, Oussaid E, Mongrain I, Lemieux Perreault LP,
622 et al. A dataset of proteomic changes during human heat stress and heat acclimation.
623 Scientific Data 2023 10:1. 2023;10: 1–6. doi:10.1038/s41597-023-02809-5
624 16. Kamel W, Noerenberg M, Cerikan B, Chen H, Järvelin AI, Kammoun M, et al.
625 Global analysis of protein-RNA interactions in SARS-CoV-2 infected cells reveals key
626 regulators of infection. Mol Cell. 2021 [cited 25 May 2021].
627 doi:10.1016/j.molcel.2021.05.023
628 17. Garcia-Moreno M, Noerenberg M, Ni S, Järvelin AI, González-Almela E, Lenz
629 CE, et al. System-wide Profiling of RNA-Binding Proteins Uncovers Key Regulators of
630 Virus Infection. Mol Cell. 2019;74: 196-211.e11. doi:10.1016/j.molcel.2019.01.017
631 18. Bonazza S, Coutts HL, Sukumar S, Turkington HL, Courtney DG. Identifying
632 cellular RNA-binding proteins during infection uncovers a role for MKRN2 in influenza
633 mRNA trafficking. Schwemmle M, editor. PLoS Pathog. 2024;20: e1012231.
634 doi:10.1371/journal.ppat.1012231
635 19. Schmidt N, Ganskih S, Wei Y, Gabel A, Zielinski S, Keshishian H, et al. SND1 binds
636 SARS-CoV-2 negative-sense RNA and promotes viral RNA synthesis through NSP9.
637 Cell. 2023;186: 4834-4850.e23. doi:10.1016/J.CELL.2023.09.002
638 20. Xia W, Su L, Jiao J. Cold-induced protein RBM3 orchestrates neurogenesis via
639 modulating Yap mRNA stability in cold stress. J Cell Biol. 2018;217: 3464–3479.
640 doi:10.1083/JCB.201801143
641 21. Lin P, Lin C, Diao L. RBM3 Ameliorates Acute Brain Injury-induced Inflammation
642 and Oxidative Stress by Stabilizing GAS6 mRNA Through Nrf2 Signaling Pathway.
643 Neuroscience. 2024;547: 74–87. doi:10.1016/J.NEUROSCIENCE.2024.03.028

644 22. Dupont M, Krischuns T, Gianetto QG, Paisant S, Bonazza S, Brault J-B, et al. The
645 RBPome of influenza A virus NP-mRNA reveals a role for TDP-43 in viral replication.
646 Nucleic Acids Res. 2024;52. doi:10.1093/NAR/GKAE291
647 23. Castello A, Fischer B, Eichelbaum K, Horos R, Beckmann BM, Strein C, et al.
648 Insights into RNA Biology from an Atlas of Mammalian mRNA-Binding Proteins. Cell.
649 2012;149: 1393–1406. doi:10.1016/j.cell.2012.04.031
650 24. Preußner M, Smith HL, Hughes D, Zhang M, Emmerichs A, Scalzitti S, et al. ASO
651 targeting RBM3 temperature-controlled poison exon splicing prevents
652 neurodegeneration in vivo . EMBO Mol Med. 2023;15. Available:
653 https://www.embopress.org/doi/10.15252/emmm.202217157
654 25. Paz I, Kosti I, Ares M, Cline M, Mandel-Gutfreund Y. RBPmap: a web server for
655 mapping binding sites of RNA-binding proteins. Nucleic Acids Res. 2014;42.
656 doi:10.1093/NAR/GKU406
657 26. Liu Y, Hu W, Murakawa Y, Yin J, Wang G, Landthaler M, et al. Cold-induced
658 RNA-binding proteins regulate circadian gene expression by controlling alternative
659 polyadenylation. Scientific Reports 2013 3:1. 2013;3: 1–11. doi:10.1038/srep02054
660 27. Ratnadiwakara M, Änkö M-L. mRNA Stability Assay Using transcription
661 inhibition by Actinomycin D in Mouse Pluripotent Stem Cells. Bio Protoc. 2018;8.
662 doi:10.21769/BIOPROTOC.3072
663 28. RB Z, XL L, CY Z, DC Y. RNA binding motif protein 3: a potential biomarker in
664 cancer and therapeutic target in neuroprotection. Oncotarget. 2017;8.
665 doi:10.18632/ONCOTARGET.14755

666 29. Serin G, Joseph G, Ghisolfi L, Bauzan M, Erard M, Amalric F, et al. Two RNA-
667 binding domains determine the RNA-binding specificity of nucleolin. J Biol Chem.
668 1997;272: 13109–13116. doi:10.1074/JBC.272.20.13109
669 30. Peretti D, Bastide A, Radford H, Verity N, Molloy C, Martin MG, et al. RBM3
670 mediates structural plasticity and protective effects of cooling in neurodegeneration.
671 Nature. 2015;518: 236–239. doi:10.1038/NATURE14142
672 31. Wellmann S, Truss M, Bruder E, Tornillo L, Zelmer A, Seeger K, et al. The RNA-
673 Binding Protein RBM3 Is Required for Cell Proliferation and Protects Against Serum
674 Deprivation-Induced Cell Death. Pediatric Research 2010 67:1. 2010;67: 35–41.
675 doi:10.1203/pdr.0b013e3181c13326
676 32. Dresios J, Aschrafi A, Owens GC, Vanderklish PW, Edelman GM, Mauro VP. Cold
677 stress-induced protein Rbm3 binds 60S ribosomal subunits, alter microRNA levels,
678 and enhances global protein synthesis. Proc Natl Acad Sci U S A. 2005;102: 1865–
679 1870. doi:10.1073/PNAS.0409764102/SUPPL_FILE/09764FIG7.JPG
680 33. Zhang D, Qiao L, Lei X, Dong X, Tong Y, Wang J, et al. Mutagenesis and structural
681 studies reveal the basis for the specific binding of SARS-CoV-2 SL3 RNA element with
682 human TIA1 protein. Nature Communications 2023 14:1. 2023;14: 1–12.
683 doi:10.1038/s41467-023-39410-8
684 34. Zhang X, Chu H, Chik KKH, Wen L, Shuai H, Yang D, et al. hnRNP C modulates
685 MERS-CoV and SARS-CoV-2 replication by governing the expression of a subset of
686 circRNAs and cognitive mRNAs. Emerg Microbes Infect. 2022;11: 519.
687 doi:10.1080/22221751.2022.2032372

688 35. Kases K, Schubert E, Hajikhezri Z, Larsson M, Devi P, Darweesh M, et al. The
689 RNA-binding protein ZC3H11A interacts with the nuclear poly(A)-binding protein
690 PABPN1 and alters polyadenylation of viral transcripts. Journal of Biological
691 Chemistry. 2023;299: 104959. doi:10.1016/j.jbc.2023.104959

692 36. Kawaguchi A, Matsumoto K, Nagata K. YB-1 Functions as a Porter To Lead
693 Influenza Virus Ribonucleoprotein Complexes to Microtubules. J Virol. 2012;86:
694 11086. doi:10.1128/JVI.00453-12

695 37. Wang K, Huang C, Jiang T, Chen Z, Xue M, Zhang Q, et al. RNA-binding protein
696 RBM47 stabilizes IFNAR1 mRNA to potentiate host antiviral activity. EMBO Rep.
697 2021;22. doi:10.15252/EMBR.202052205

698 38. Thul PJ, Akesson L, Wiking M, Mahdessian D, Geladaki A, Ait Blal H, et al. A
699 subcellular map of the human proteome. Science (1979). 2017;356.

700 39. Schmid M, Jensen TH. The exosome: a multipurpose RNA-decay machine.
701 Trends Biochem Sci. 2008;33: 501–510. doi:10.1016/j.tibs.2008.07.003

702 40. Yang R, Pan M, Guo J, Huang Y, Zhang QC, Deng T, et al. Mapping of the
703 influenza A virus genome RNA structure and interactions reveals essential elements
704 of viral replication. Cell Rep. 2024;43. doi:10.1016/J.CELREP.2024.113833

705 41. Courtney DG, Kennedy EM, Dumm RE, Bogerd HP, Tsai K, Heaton NS, et al.
706 Epitranscriptomic Enhancement of Influenza A Virus Gene Expression and
707 Replication. Cell Host Microbe. 2017;22: 377–386. doi:10.1016/j.chom.2017.08.004

708 42. Vale-Costa S, Etibor TA, Brás D, Sousa AL, Ferreira M, Martins GG, et al. ATG9A
709 regulates the dissociation of recycling endosomes from microtubules to form liquid

710 influenza A virus inclusions. PLoS Biol. 2023;21: e3002290.
711 doi:10.1371/JOURNAL.PBIO.3002290

712 43. Morens DM, Taubenberger JK, Fauci AS. Rethinking next-generation vaccines
713 for coronaviruses, influenzaviruses, and other respiratory viruses. Cell Host Microbe.
714 2023;31: 146–157. doi:10.1016/J.CHOM.2022.11.016

715 44. Sheikh-Mohamed S, Isho B, Chao GYC, Zuo M, Cohen C, Lustig Y, et al. Systemic
716 and mucosal IgA responses are variably induced in response to SARS-CoV-2 mRNA
717 vaccination and are associated with protection against subsequent infection.
718 Mucosal Immunol. 2022;15: 799. doi:10.1038/S41385-022-00511-0

719 45. Liew F, Talwar S, Cross A, Willett BJ, Scott S, Logan N, et al. SARS-CoV-2-specific
720 nasal IgA wanes 9 months after hospitalisation with COVID-19 and is not induced by
721 subsequent vaccination. EBioMedicine. 2023;87: 104402.
722 doi:10.1016/J.EBIOM.2022.104402

723 46. Fodor E, Devenish L, Engelhardt OG, Palese P, Brownlee GG, García-Sastre A.
724 Rescue of Influenza A Virus from Recombinant DNA. J Virol. 1999;73: 9679.
725 doi:10.1128/JVI.73.11.9679-9682.1999

726 47. Courtney DG, Chalem A, Bogerd HP, Law BA, Kennedy EM, Holley CL, et al.
727 Extensive epitranscriptomic methylation of A and C residues on murine leukemia
728 virus transcripts enhances viral gene expression. mBio. 2019;10: e01209-19.
729 doi:http://dx.doi.org/10.1101/591545

730 48. Queiroz RML, Smith T, Villanueva E, Marti-Solano M, Monti M, Pizzinga M, et
731 al. Comprehensive identification of RNA–protein interactions in any organism using

732 orthogonal organic phase separation (OOPS). Nature Biotechnology 2019 37:2.
733 2019;37: 169–178. doi:10.1038/s41587-018-0001-2
734 49. Cox J, Mann M. MaxQuant enables high peptide identification rates,
735 individualized p.p.b.-range mass accuracies and proteome-wide protein
736 quantification. Nature Biotechnology 2008 26:12. 2008;26: 1367–1372.
737 doi:10.1038/nbt.1511
738 50. Tyanova S, Temu T, Sinitcyn P, Carlson A, Hein MY, Geiger T, et al. The Perseus
739 computational platform for comprehensive analysis of (prote)omics data. Nature
740 Methods 2016 13:9. 2016;13: 731–740. doi:10.1038/nmeth.3901
741 51. Courtney DG, Tsai K, Bogerd HP, Kennedy EM, Law BA, Emery A, et al.
742 Epitranscriptomic Addition of m5C to HIV-1 Transcripts Regulates Viral Gene
743 Expression. Cell Host Microbe. 2019;26: 217–227. doi:10.1016/j.chom.2019.07.005
744 52. Kawakami E, Watanabe T, Fujii K, Goto H, Watanabe S, Noda T, et al. Strand-
745 specific real-time RT-PCR for distinguishing influenza vRNA, cRNA, and mRNA. J Virol
746 Methods. 2011;173: 1. doi:10.1016/J.JVIROMET.2010.12.014
747 53. Broadbent L, Villenave R, Guo-Parke H, Douglas I, Shields MD, Power UF. In
748 Vitro Modeling of RSV Infection and Cytopathogenesis in Well-Differentiated Human
749 Primary Airway Epithelial Cells (WD-PAECs). Methods Mol Biol. 2016;1442: 119–139.
750 doi:10.1007/978-1-4939-3687-8_9
751
752

753 **Supplementary data**

754 Supplementary Table 1 – Initial RIC dataset prior to downstream analysis

755 Supplementary Table 2 – RIC dataset of RBP identified in at least 2 replicates of each

756 condition, with fold enrichment and p values included.

757 Supplementary Table 3 – siRNA sequences

758 Supplementary Table 4 – Primer sequences

759 Supplementary Table 5 – Sequences of antisense oligonucleotides

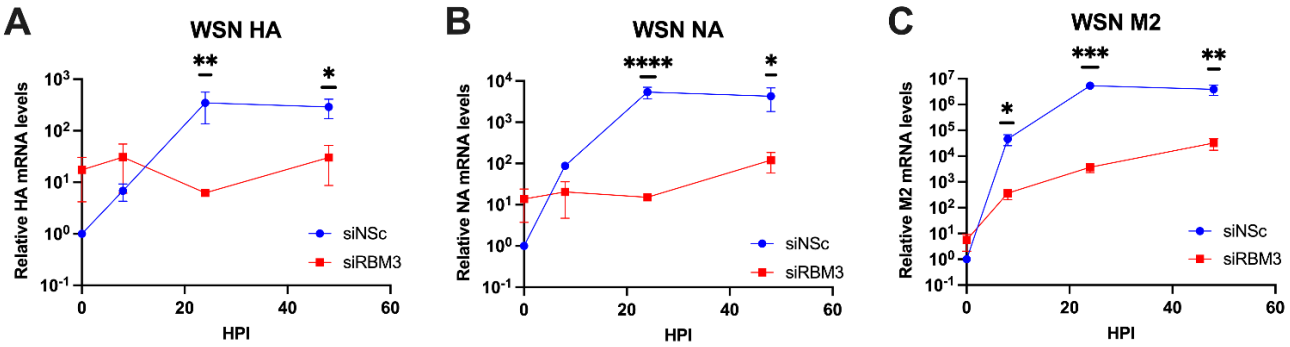

760

761 Supplementary Figure 1 – Growth curve of WSN replication quantified by viral transcript levels

762 Viral transcripts HA (A), NA (B) and M2 (C) were quantified in siRNA transfected A549 cells

763 infected with WSN at MOI 0.01 at 0, 8, 24 and 48 hpi. Cells treated with an RBM3 targeting

764 siRNA (siRBM3) for 48 h prior to infection demonstrated diminished transcript levels

765 compared to a negative control (siNSC) siRNA.